Cellular Oncology (2025) 48:693–708
https://doi.org/10.1007/s13402-025-01040-1

RESEARCH

# Tumor-specific CXCR6 positive precursor CD8$^+$ T cells mediate tumor control in metastatic melanoma

Yang Song[1] · Ji Chen[1] · Yaqin Zhang[1] · Ning Wu[1] · Yongjun Zhu[1] · Gang Chen[1] · Feng Miao[1] · Zhiming Chen[1] · Yiqing Wang[1]

Accepted: 16 January 2025 / Published online: 7 April 2025


## Abstract

**Background** Adoptive cell therapy (ACT) mediates durable and complete regression of various cancers. However, its efficacy is limited by the long-term persistence of cytotoxic T lymphocytes, given their irreversible dysfunction within the tumor microenvironment. Herein, we aimed to establish an artificial lung metastasis model to examine T-lymphocyte subsets, in order to identify potential effective cell subsets for ACT.

**Methods** A metastatic lung melanoma mouse model was established using OVA-expressing melanoma B16 cells. Flow cytometry analysis was conducted to examine the surface markers, transcription factors, and secreted cytokines of tumor-specific CD8$^+$ T cells within metastatic tissues. The infiltrated cells were sorted by flow cytometry for in vitro tumor cell killing assays or in vivo cell infusion therapy combined with chemotherapeutic drugs and immune checkpoint blockade antibodies.

**Results** Exhausted CD8$^+$ T cells (Tex) exhibited high heterogeneity in metastatic tissues. Among Tex cells, the CXCR6$^-$ precursor cell showed certain memory characteristics, including phenotype, transcription factors, and maintenance, whereas the CXCR6$^+$ subpopulation partially lost these traits. Moreover, CXCR6$^+$ precursor cells effectively replenished effector-like Tex cells in metastatic tissues and exerted direct cytotoxicity against tumor cells. Notably, transferring these tumor-specific CXCR6$^+$ precursor-exhausted T (Texp) cells into recipients induced a substantial regression of metastasis. In addition, these cells could respond to immune checkpoint blockade, which could better control tumor metastasis.

**Conclusions** In our study, a subset of antigen-specific CXCR6-expressing Texp cells was observed within the metastatic tissue. The cells served as a crucial source of effector-like Tex cells and exerted direct cytotoxic effects on tumor cells. Adoptive transfer of CXCR6$^+$ Texp cells effectively mitigated lung metastasis in mice. This study helps elucidate the role of Texp cells in metastasis, thereby offering novel insights into enhancing the efficacy and durability of immunotherapy.

**Keywords** Metastasis · Tumor-specific · CXCR6$^+$precursor exhausted T cell · Immunotherapy

**Abbreviations**

| | |
|---|---|
| ACT | Adoptive cell therapy |
| CTL | Cytotoxic T lymphocytes |
| Tex | Exhausted CD8$^+$ T cells |
| ICB | Immune checkpoint blockade |
| PD-1/PD-L1 | Programmed cell death protein 1 and its ligand |
| Texp | Precursor-exhausted T cells |
| MLN | Mediastinal lymph nodes |
| CTX | Cyclophosphamide |
| DC | Dendritic cell |

Yang Song, Ji Chen and Yaqin Zhang contributed equally.

✉ Zhiming Chen
chzm_md@163.com

✉ Yiqing Wang
wangyiqing@huashan.org.cn

[1] Department of Cardio-Thoracic Surgery, Huashan Hospital, Fudan University, Shanghai, China

## 1 Background

Metastasis is the leading cause of cancer-related mortality and a significant barrier to curative therapies [1]. Traditional clinical approaches such as surgery and radiotherapy

often fail to treat tumor metastasis. To overcome this limitation, adoptive cell therapy (ACT) using autologous T cells has been proposed. ACT involves the infusion of in vitro expanded tumor-specific cytotoxic T lymphocytes (CTLs), that have been associated with remarkable remission rates in patients [2, 3]. However, a major obstacle to ACT is the susceptibility of infused CTLs to exhaustion within the inhibitory tumor microenvironment [4].

Exhausted $CD8^+$T (Tex) cells are characterized by an elevated expression of inhibitory receptors, impaired proliferative potential, loss of effector functions, and distinct transcriptional and epigenetic profiles compared to effector or memory cells [5–7]. Immune checkpoint blockade (ICB), targeting the programmed cell death protein 1 and its ligand (PD-1/PD-L1) pathway with monoclonal antibodies, has been approved for the treatment of various cancer types, and has been associated with improved tumor regression and patient survival rates [8].

However, despite combining ICB with first-line platinum-doublet chemotherapy [9], more than half of the treated patients fail to respond. In reality, prior to ICB emerging as a significant modality for cancer treatment, tumor-infiltrating $CD8^+$T cells had already been acknowledged as a crucial factor in governing prognosis. Additionally, researchers have endeavored to employ ICB in combination with autologous tumor-infiltrating lymphocyte infusion for immunotherapy of non-small cell lung cancer patients, and have attained potentially therapeutic outcomes [10]. Recent studies have revealed heterogeneity among Tex cells [11–13]. Precursor-exhausted T (Texp) cells express stemness-related transcription factors such as TCF-1 and give rise to the Tim3-expressing terminal Tex subset in chronic infections and tumors [14–16]. Furthermore, the response of precursor populations to checkpoint blockade has been reported [17, 18]. However, the immunological characteristics and functions of Texp cells during metastasis are poorly understood.

Herein, we aimed to establish an artificial lung metastasis model using a melanoma cell line. Using flow cytometry, we observed a subset of antigen-specific CXCR6-expressing Texp cells within the metastatic tissue. They displayed limited molecular characteristics associated with memory, combined with prompt replenishment into effector-like Tex cells, and exerted direct cytotoxic effects on tumor cells. Adoptive transfer of $CXCR6^+$ Texp cells effectively mitigated lung metastasis in mice, and when combined with chemotherapy or ICB, further augmented treatment efficacy. This study provides novel insights for the clinical treatment of ACT.

## 2 METHODS

### 2.1 Mice

C57BL/6J, $Cd8^{-/-}$ mice, CD45.1 congenic mice, $Cxcr6^{-/-}$ and OT-I TCR transgenic mice were purchased from the Jackson Laboratories. We crossed $Cxcr6^{-/-}$ mice with OT-I mice to generate mice in which the *Cxcr6* alleles are deleted in $CD8^+$ T cells (hereafter referred to as $Cxcr6^{-/-}$ OT-I mice). Approximately 6-10-week old mice of both sexes were engrafted with tumor cells without randomization or "blinding". All Mice were bred in pathogen free conditions. Mice dying for nonrelated cancer causes were excluded from the studies (i.e., fights or infections). Mice were performed with the guidelines of the Institutional Animal Care and Use Committees at The HuaShan Hospital, Fudan University.

### 2.2 Experimental lung metastasis model

Mouse melanoma B16(F10) cells and $B16^{luc}$ cells (B16 transduced with firefly luciferase) were obtained from ATCC, B16-$OVA^{luc}$ cells (B16 stably expressing chicken OVA peptide) were developed in our lab. All the transgenic melanoma cells utilized in this research originated from the parent cell line B16(F10), and the cells were cultured in DMEM (Gibco) supplemented with 2nM L-glutamine, 1nM penicillin/ streptomycin and 10% (v/v) FBS. All cell lines were tested routinely prior to use to exclude mycoplasma contamination. The spontaneous metastasis mouse model was established following the published protocol [19]. In brief, an inoculum dose of $5 \times 10^5$ of melanoma cells in 0.3 ml PBS were subcutaneously injected into the footpad. After 10–14 days, tumor growth in the footpad was measured with calipers until the tumor reached approximately $0.8 \times 0.8$ cm in diameter. Subsequently, the mice were anesthetized, and the leg bearing the tumor was amputated. The feasibility of the model was evaluated by analyzing the fluorescence signals in the mouse lung via live imaging detection. Additionally, after mice have received ACT treatment, count the number of lung nodules(black/opaque foci) with the aid of a dissection microscope at the different indicated time.

To analyze the immunologic characteristics of tumor-specific $CD8^+$ T cells, we mimicked the formation of metastatic in lung tissue from melanoma. Total $3 \times 10^5$ of melanoma cells in 0.5 ml PBS were intravenously through the tail vein. A total of approximately $5 \times 10^5$ of naïve splenic $CD8^+$ T cells from $CD45.1^+$ OT-I transgenic mice were adoptively transferred to the tumor bearing mice ($CD45.2^+$) through the tail vein. The purification of $CD8^+$ T cells was performed by using mouse $CD8^+$ T cells isolation kit (StemCell Technologies) according to manufacturer's protocol. The OT-I

cells analyzed or sorted in this study were all gated from the CD44$^+$ population. In immunotherapeutic experiments, total of $5\times10^5$ Slamf6$^+$CXCR6$^+$ OT-I cells derived from metastatic donor mice were adoptively transferred to the recipient mice, which were inoculated with B16-OVA cells intravenously or subcutaneously on the following day. In addition, the recipient mice that received ACT treatment did not undergo lymphodepletion using any pharmacological agents.

### 2.3 Development of subcutaneous tumor and virus infection models

For subcutaneous tumor model development, total $6\times10^5$ B16-OVA cells were injected subcutaneously in the inguinal angle of mice. All subcutaneous and pulmonary tumor measurements were performed in a blinded manner. To ensure consistency, preparation of the cells, measure the tumor size, administration into the tail vein and counting of pulmonary metastatic foci were performed by the same individual. To establish acute viral infection and harvest tissue-resident memory CD8$^+$T cells (Trm) residing in lung tissue, mice were anesthetized by i.p. injection of 2,2,2-tribromoethanol following the intranasal influenza virus A/HK-x31-OVA infection at 300 50% egg infectious doses (EID50). The recombinant influenza virus have been previously described (Shiki Takamura, 2010).

### 2.4 Mouse tissue harvesting and digest

Spleens or lung-draining mediastinal lymph nodes (MLNs) were surgically removed and crushed with grinding rod on petri dishes containing red blood cell lysis buffer. The cell mixtures were then centrifuged at 1500 rpm for 5 min following resuspension in RPMI-1640 media containing 5% FBS (w/v). To prepare cell suspensions in lung metastases, mice was intravenously injected 2 μg per mice anti-CD8(APC-cy7, Biolegend) before sacrifice in order to eliminate circulatory CD8$^+$ T cells in peripheral blood. The lungs were dissected out carefully, and then wash the tissue gently though cardiac perfusion with PBS. Then lungs were minced mechanically following digest using type-II collagenase (Sigma) for 30 min at 37$^o$C. Finally, tissue-infiltrated lymphocytes were harvested using density gradient (2200 rpm, 40 min) with Percoll (GE Healthcare). Obtained cells were stained with anti-CD8(PercpCy5.5, BD Biosciences) and lung-resident CD8$^+$ T cells were referred as PercpCy5.5 positive and APC-cy7 negative.

### 2.5 In vivo antibody treatment

After OT-I cells transfer, metastatic mice was intraperitoneally administrated with αPD-1(150 μg, BioXCell) or rat IgG2b control antibody (150 μg, BioXCell) on indicated time points. For IL15 and TGFβ cytokines blocking in vivo, 150 μg of anti-IL15 (BioXCell) or anti-TGFβ (BioXCell) and isotype-matched control antibody were intraperitoneally treated to mice on day 3, 6 and 9 post cells transfer.

### 2.6 In vitro cell culture and stimulation

The Slamf6$^+$ OT-I cells were sorted from lung tissues of metastasis mice. Single cell suspensions(approximately $1\times10^5$) were resuspended in complete RPMI-1640 medium (containing 10%(v/v) FBS, 2nM L-Glutamine and 1nM penicillin/streptomycin) and added to CD3(0.2 mg/ml), CD28(0.1 mg/ml) mAbs-coated culture plates, in the presence of IL2(20ng/ml) for 48 h prior to evaluation by flow cytometry.

### 2.7 In vitro killing assay

Splenic singe cell suspension from C57BL/6J mice (CD45.2$^+$) was prepared firstly, T cells were eliminated by negative selection. Residual cells were labeled with CellTrace CFSE (Thermo Fisher) at the title of either 1 mM or 100 nM for 30 min at room temperature in the dark. Next, CFSE-high labeled cells were pulsed with $OVA_{257-264}$ peptide(5 mg/ml) for 2 h at 37 °C, in contrast, CFSE-low labeled cells with $OVA_{323-339}$ peptide (not recognized by OT-I cells) as control. High- or low-level labeled cells were mixed at a ratio of 1:1, subsequently co-culture with CXCR6$^+$ OT-I cells purified from metastasis mice for 12 h at 37 °C.

### 2.8 Live imaging detection

For detection of metastasis progression without sacrifice mice, recipient mice bearing B16$^{luc}$ cells were intraperitoneally treated with 3 mg D-luciferin K$^+$ salt(Goldbio) prior to gaseous anesthesia. Luciferin image was obtained and analyzed using IVIS LuminaII system(Xenogen).

### 2.9 Flow cytometry analysis

The antibodies and reagents in experiments as shown in Supplementary Table 1. For surface staining, cells were firstly stained with anti-CD16/CD32 antibody(Thermo Fisher) on ice for 30 min, after cleaning twice with wash buffer (1% BSA in PBS), cells were stained with LIVE/DEAD dye(Thermo Fisher) and surface marker antibodies at 4$^o$C for 30 min. For

cytokine production test, lymphocytes were stimulated in the presence of 0.2 μg/ml of $OVA_{257-264}$ peptide and 50ng/ml of phorbol myristate acetate (PMA), ionomycin (1 μg/ml, Sigma) supplemented with GolgiPlug/stop (BD Biosciences) for 4 h at 37ºC, then harvested the lymphocytes following surface staining and intracellular cytokine staining with Cytofix/Cytoperm Fixation/permeabilization Kit (BD Biosciences). Intracellular and intranuclear antibodies were incubated for 30 min at room temperature. The counting beads (Thermo Fisher) was added to the samples to acquisition the absolute number of cells. In the assay of in vivo incorporation of the thymidine analog BrdU, recipient mice were intraperitoneally injected with BrdU (1.5 mg/mice) for four times before mice were sacrificed. BrdU staining was performed with a BrdU Flow Kit (BD Biosciences) according to the manufacturer's instructions. Flow cytometry data were collected with a FACSCanto II (BD Biosciences) and analyzed by using FlowJo software (TreeStar).

### 2.10 Bone marrow chimeras

Bone marrow was collected from the femur and tibia of C57BL/6J, *Cd8*$^{-/-}$ and *Cxcr6*$^{-/-}$mice into sterile RPMI-1640 media. Fifty-fifty mixture of bone marrow cells was pelleted by centrifugation at 1500 rpm for 5 min, then filtered through a 70 mm cell strainer and resuspended in sterile PBS. Approximately $1 \times 10^7$ of cells were intravenously injected into lethally irradiated recipient mice (two doses of 550 rad, three hours apart). Recipient mice were allowed hematopoietic reconstitution for at least 8 weeks prior to tumor transplantation.

### 2.11 Quantitative reverse-transcription PCR

OT-I cells were adoptively transfer to mice one day prior to recombinant influenza virus infection, Trm cells marked by CD103 and CD69 double positive were sorted on day 40 by using a fluorescence-activated cells sorting(FACS) Aria III (BD Biosciences). In addition, the tumor-specific precursor OT-I cells which infiltrated in the lung of metastatic mice were harvested using FACS. Total RNA was isolated from cells using RNeasy Mini Kit (Qiagen), and reverse transcribed into first-strand complementary DNA (cDNA) with PrimeScript™ RT reagent Kit(Takara). Then, the samples were analyzed in the Applied Biosystems QuantStudio 3 Real-Time PCR system(Thermo Fisher). Information about the primers was listed in Supplementary Table 2.

### 2.12 Statistical analysis

For normally distributed data, significance of mean differences was determined using one-way ANOVA or unpaired t-tests. In case of correlations, the Pearson correlation was used to test statistical significance. Survival data were performed as Kaplan-Meier survival curves with the log-rank test. Error bars shown in graphical data represent mean ± s.d. A two-tailed value of $P < 0.05$ was considered statistically significant. All statistical analyses were performed using GraphPad Prism v.8.0.

## 3 Results

### 3.1 Tex cells show high heterogeneity and distinct efficacy in alleviating lung metastasis

To investigate the response of tumor-infiltrating CTLs to metastatic tumors, we used an experimental mouse model of lung melanoma metastasis [18]. B16$^{luc}$ cells (harboring a luciferase-coding gene) were inoculated into footpad of mice and subsequent metastatic foci in the lungs were observed in proportion to the intensity of the luciferase reporter signal (Fig. 1a). Consequently, we aimed to investigate whether the adoptive transfer of antigen-specific CD8$^+$ T cells could mitigate metastatic tumors. Prior to surgical resection of the primary tumor, mice with confirmed lung metastases were subjected to a luciferase assay. To eliminate the potential influence of endogenous CD8$^+$ T cells, we selected CD8$^+$ T cell-depleted (*Cd8*$^{-/-}$) mice as hosts. Despite this, the fluorescence signal intensity in the lung tissue of *Cd8*$^{-/-}$ mice did not significantly differ from that of wild-type mice at various time points (supplemental figure S1a). A total of $10 \times 10^5$ naïve or activated splenic OT-I cells ($OVA_{257-264}$ I-A$^b$- specific) were adoptively transferred intravenously into *Cd8*$^{-/-}$ mice bearing lung metastases (Fig. 1b). Mice receiving activated OT-I cells instead of naïve cells showed significantly enhanced survival rates compared with controls, indicating that the transfer of activated antigen-specific CD8$^+$ T cells is highly efficacious in controlling metastasis.

The differentiation pattern of antigen-specific CD8$^+$ T cells in the tumor microenvironment has been previously investigated [11]. However, there is a limited understanding of this phenomenon in the context of metastatic tissue. A total of $5 \times 10^5$ splenic CD45.1$^+$OT-I cells were intravenously administered to mice on day −2, followed by intravenous inoculation with B16-OVA cells (B16 cells expressing the $OVA_{257-264}$ peptide). Subsequently, the lung tissue was harvested, and the infiltrated CD44$^+$OT-I cells were analyzed using flow cytometry. Whole tissue-infiltrating OT-I cells were classified into Texp cells (TCF1$^+$Tim3$^-$ CX3CR1$^-$), transitory effector-like Tex cells (TCF1$^-$CX3CR1$^+$), and terminal Tex cells (TCF1$^-$Tim3$^+$CD101$^+$) (supplemental figure S1b). Notably, we observed an initial predominance of Texp

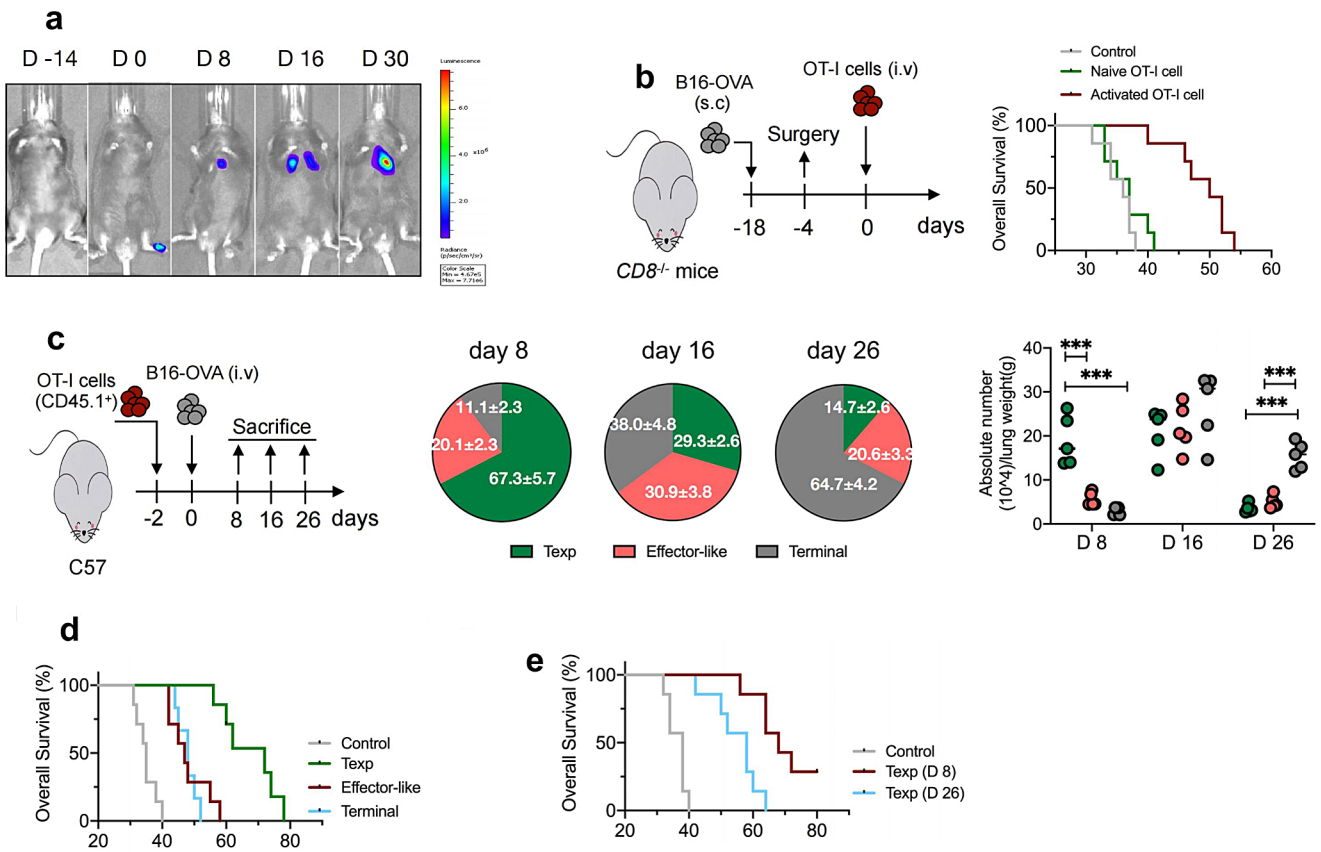


**Fig. 1** Differentiation pattern of OT-I cells within metastatic tissues and therapeutic outcome of ACT (**a**). Approximately $5\times10^5$ of $B16^{luc}$ cells expressed luciferase were subcutaneously injected into the footpad of C57BL/6J mice to develop the spontaneous lung metastasis mice model, luciferin was administrated on day 0, 8, 16, 30, and light emission was recorded. Representative bioluminescence images are shown. (**b**). $Cd8^{-/-}$ mice were subcutaneously injected with B16-OVA cells, after 14 days, lung-metastasis mice were confirmed by luciferase assay prior to surgery. Totally $1\times10^6$ of naïve splenic OT-I cells or activated OT-I cells that were derived from stimulation with anti-CD3/CD28 and IL-2 in vitro were i.v adoptively transferred into mice. No treatment mice were used as control. Survival curve of mice was calculated. Red line versus gray line, $p<0.01$; Green versus gray line, $p=0.33$; log rank test was used. (**c**). Naïve splenic OT-I cells ($5\times10^5$, $CD45.1^+$) were transferred into C57BL/6J mice ($CD45.2^+$, $n=5$ per group) subsequently injection with B16-OVA cells ($3\times10^5$) via tail vein. On day 8, 16 and 26 post transfer, lungs were harvested and tissue-infiltrating lymphocytes (TILs) were isolated and subjected to flow cytometry. Frequency and absolute number of precursor-exhausted (Texp), effector-like and terminal Tex subsets of OT-I cells were measured. Statistical comparisons were performed using an unpaired t-test, $^{***}p<0.001$. Data are shown as the mean±s.e.m. (**d**). Approximately $1\times10^6$ of lung-derived Tex cells that were sorted from donor mice on day 12 as described in (**c**), or isolated Texp cells on day 8 or day 26 (**e**), were adoptively transferred into pre-established metastasis-bearing $Cd8^{-/-}$ mice 4 days post-surgery. Survival curve of mice was calculated. In (**d**), Blue / red line versus gray line, $p<0.01$; Green versus blue / red line, $p<0.01$; In (**e**), Blue line versus gray line, $p<0.01$; Red line versus blue line, $p=0.015$. log rank test was used

cells among expanded antigen-specific $CD8^+$ T cells, which gradually declined thereafter. In addition, there was a 3- to 5-fold increase in the proportion of terminal Tex cells at the examined time points, whereas the effector-like Tex cell population exhibited only marginal fluctuations during metastatic progression (Fig. 1c). These findings demonstrated that tumor-specific $CD8^+$ T cells exhibit high heterogeneity in exhaustion within metastatic tissues.

Co-expression of TCF1 and Slamf6 was prominently observed in tumor-reactive $CD8^+$T cells in the lungs, in line with the notion that Slamf6 functions as a representative molecule for Texp cells in chronic infections or tumor models [12] (supplemental figure S1c). Based on these findings, we hypothesized that activated $CD8^+$ T-cells may play a crucial role in the regulation of metastasis. To further investigate this phenomenon, we isolated lung-derived tumor-specific effector-like Tex cells, based on the expression of the surface molecule $Slamf6^-CX3CR1^+$, and subsequently re-transferred them into $Cd8^{-/-}$ mice bearing metastases for therapeutic purposes. In addition, we concurrently processed Texp cells (identified as $Slamf6^+Tim3^-$) and terminal Tex cells (characterized as $Slamf6^-CD101^+$). Our findings revealed that the transfer of tumor-specific effector-like Tex cells did not confer any survival advantage; however, the administration of Texp cells resulted in remarkable remission of metastasis (Fig. 1d). Moreover, the

infusion of precursor cells at different time points yielded distinct advantages in terms of the overall survival duration for mice with metastases (Fig. 1e). Collectively, these findings support the essential role of Texp cells derived from metastatic tissues in protecting against the invasion of metastatic lesions.

### 3.2 CXCR6$^+$ subsets are present in Texp cells

Subsequently, we examined the distinctive characteristics exhibited by tumor-specific Texp cells during metastasis. Chemokine receptors play a crucial role in mediating CD8$^+$ T-cell responses against tumors [20–23]; therefore, we examined their relative expression in metastatic tissues. A total of $5\times10^5$ CD45.1$^+$OT-I cells were transferred to mice on day −2, after the intravenous administration of B16-OVA cells, lung tissues were harvested and subjected to CD44$^+$OT-I cell analysis on the indicated days. To eliminate potential contamination from circulating CD8$^+$ T cells in the peripheral blood, mice were intravenously administered anti-CD8 (APC-cy7 channel) prior to sacrifice, enabling the identification of lung-resident CD8$^+$ T cells that lacked APC-cy7 staining. Notably, we observed a subset of Texp cells with pronounced upregulation of CXCR6 but lacking obvious expression of CCR2, CXCR3, CXCR5, or CX3CR1; however, this expression gradually declined at subsequent time points (Fig. 2a) (supplemental figure S2a). Moreover, a comparable expression pattern was observed in endogenous tumor-reactive CD8$^+$ T cells (identified as $OVA_{257-264}$ peptide (SIINFEKL) H-2K$^b$ tetramer-positive) within metastatic mice (supplemental figure S2b). However, the number of CXCR6$^+$ Texp cells within the subcutaneous tumors was limited (supplemental figure S2c).

Recent studies have revealed the crucial role of tumor-draining lymph nodes in facilitating CD8$^+$ T cell infiltration into the solid tumor microenvironment [24–26]. We aimed to investigate whether tissue-derived CXCR6$^+$ Texp cells could migrate from lung-draining mediastinal lymph nodes (MLNs). Given that surgical resection of MLNs is challenging, we opted for a pharmacological intervention using FTY720 to effectively impede cell migration from MLNs to the peripheral blood. Mice were adoptively transferred to OT-I cells, followed by inoculation with B16-OVA cells. Intraperitoneal administration of FTY720 was performed three times. Notably, administration of FTY720 significantly attenuated the absolute count of CXCR6$^+$ Texp cells in the lungs (Fig. 2b), highlighting the pivotal role of MLNs as a source of Texp cells during metastasis. Moreover, we investigated whether tumor antigen burden accounted for the generation of the CXCR6$^+$ population. Our findings

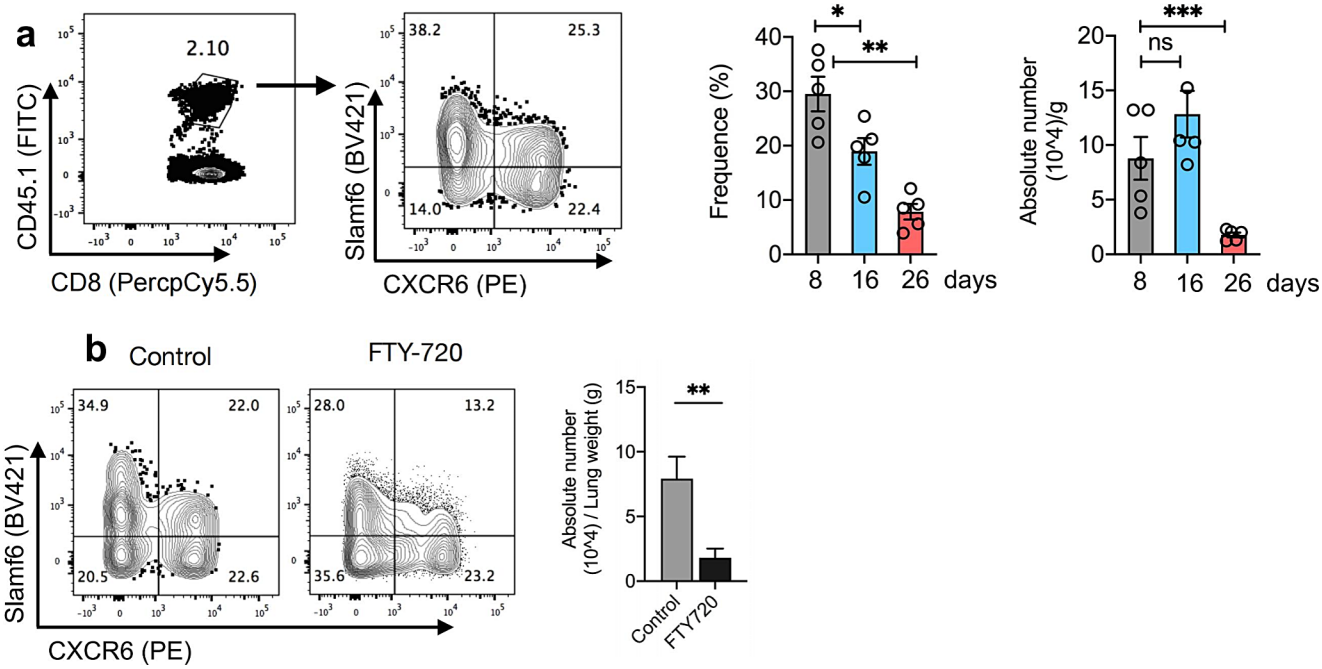


**Fig. 2** Expression pattern of CXCR6$^+$ Texp cells (**a**). C57BL/6J mice were intravenously(i.v) injected with $5\times10^5$ of CD45.1$^+$ OT-I cells prior to B16-OVA cells inoculation ($n=5$ per group), on day 8, 16 and 26, lung-derived TILs were analyzed by flow cytometry. Representative flow cytometry staining (left) and summary (right) of Slamf6/CXCR6 expression on OT-I cells (gated from live CD45.1$^+$CD44$^+$) were calculated. (**b**). CD45.1$^+$ OT-I cells ($5\times10^5$) were adoptively transferred into C57BL/6J mice ($n=4$ per group) on day −2, followed by $3\times10^5$ of B16-OVA cells inoculation. From day 3 to day 7 post transfer, mice were intraperitoneally (i.p) treated with FTY720 at a dose of 2.5 mg/kg every 2 days. Lung-derived TILs were subjected to flow cytometry, the absolute number of Slamf6$^+$CXCR6$^+$ OT-I cells were measured. In (**a**, **b**), statistical comparisons were performed using an unpaired t-test, ns, no significance, *$p<0.05$, **$p<0.01$, ***$p<0.001$. Data are shown as the mean±s.e.m. and representative of two independent experiments

revealed an elevated proportion of these cells in response to high tumor cell engraftment in lung tissues (supplemental figure S2d), implying an antigen-driven mechanism underlying CXCR6$^+$ Texp cell generation.

### 3.3 CXCR6$^+$ Texp cells exhibit limited cellular memory attributes

Texp cells have been reported to exhibit nonclassical memory cell characteristics within the tumor microenvironment [27, 28]. A total of $5 \times 10^5$ CD45.1$^+$ OT-I cells were adoptively transferred into mice prior to inoculation with B16-OVA cells. Subsequently, the lung tissue was harvested and expanded Texp cells were subjected to flow cytometric analysis. We observed that CXCR6$^+$ subsets exhibited significantly lower levels of memory-associated markers CD62L, IL2Rβ, or IL7Rα in comparison to CXCR6$^-$ cells on day 12 post-cell transfer (Fig. 3a). In addition, we investigated the expression profiles of inhibitory markers, including PD-1, Tim3, Lag3, CD39 and Tox, in tumor-specific CXCR6$^+$ Texp cells, and terminal Tex cells. These distinctive marker expressions were observed in nearly all terminal Tex cells but were absent in CXCR6$^+$ cells (Fig. 3b).

The long-term persistence of memory CD8$^+$ T cells orchestrated by homeostatic proliferation represents a fundamental mechanism that has been demonstrated to affect the establishment of anti-reinfection or anti-tumor immunity [29, 30]. To assess the long-term potential, metastatic lung tissues were harvested and Texp cells were isolated by flow cytometry. Subsequently, CXCR6$^+$ cells (CD45.1$^+$CD45.2$^+$) and CXCR6$^-$ cells (CD45.1$^+$) were co-transferred into recipient mice with a CD45.2$^+$ background at a 1:1 ratio. After resting for 14 days, the samples displayed a significant decrease in the proportion of CXCR6$^+$ cells (Fig. 3c), indicating that tumor-reactive CXCR6$^-$ Texp cells exhibit greater longevity and sustainability, whereas this function is diminished in CXCR6$^+$ cells. In addition, to elucidate the transcriptional profiles, we employed flow cytometry to sort lung-infiltrated Texp cells from mice with metastasis and Trm cells (identified by CD69$^+$CD103$^+$) from mice infected with the influenza virus. Subsequently, genotypic expression was examined by real-time qPCR analysis. Our findings revealed that CXCR6$^-$ Texp cells exhibited comparable levels of gene expression encoding signature transcription factors associated with Trm cells, such as *Runx3*, *Tcf7*, *Sell*, whereas CXCR6$^+$ cells showed a weak expression pattern (Fig. 3d).

We investigated the essentiality of IL-15 and TGFβ, two important cytokines for maintaining memory CD8$^+$ T cells, in regulating the functionality of CXCR6$^+$ Texp cells during metastasis. Prior to melanoma cell inoculation, naïve OT-I cells were adoptively transferred into mice, followed by the administration of blocking antibodies against IL-15 and TGFβ, administered three times. Lung-derived Texp cells were analyzed using flow cytometry. Treatment with both anti-IL15 and anti-TGFβ resulted in a significant reduction in the absolute number of CXCR6$^-$ Texp cells, however, the number of CXCR6$^+$ Texp cells was scarcely affected (supplemental figure S3a). Collectively, these findings suggest that tumor-specific CXCR6$^-$ Texp cells may possess a memory-like imprint characterized by specific phenotypes, transcription factors, and self-renewal capacity; however, these characteristics are predominantly diminished in the context of metastasis among CXCR6$^+$ Texp cells.

### 3.4 Generation of effector-like Tex cells predominantly relied on CXCR6$^+$ Texp cells in metastasis

We investigated the role of Texp cells in metastasis. Approximately $5 \times 10^5$ OT-I cells were adoptively transferred into mice, followed by the intravenous inoculation of B16-OVA cells. On day 8 post-cell transfer, the lungs were harvested, and Texp cells were isolated using flow cytometry. After stimulation with the $OVA_{257-264}$ peptide in vitro, along with anti-CD28 and IL-2 for 48 h, CXCR6$^+$ Texp cells exhibited a robust proliferative response (supplemental figure S4a), indicating their potential for rapid cell differentiation. Purified CXCR6$^+$ Texp cells were re-transferred into metastasis-matched mice, where a fraction (20–40%) of donor cells differentiated into CX3CR1-expressing effector-like Tex cells at the initial time point examined in the lungs; however, only a few terminal Tex counterparts were detected (Fig. 4a). Subsequent analysis revealed a significant increase in the frequency of terminal Tex subsets and a gradual decrease in the number of newly formed effector-like Tex cells. These findings suggest that CXCR6$^+$ Texp cells can promptly replenish the early population of effector-like Tex cells during metastatic progression.

To validate the replenishment of effector-like Tex subsets in metastatic tissues, we performed an in vivo cell co-transfer assay. Lung-derived CXCR6$^+$/CXCR6$^-$ Texp cells from different donors were sorted by flow cytometry and co-transferred in a 1:1 ratio into recipient mice with matched metastases. On day 6 post-cell transfer, more than half of the CXCR6$^+$ cells underwent differentiation into effector-like Tex counterparts, whereas most donor CXCR6$^-$ cells exhibited sustained Slamf6 expression (Fig. 4b). In addition, CD45.1$^+$*Cxcr6*$^{-/-}$ and CD45.1/2$^+$*Cxcr6*$^{+/+}$ OT-I cells were co-transferred in equal numbers into naïve mice, followed by inoculation with B16-OVA cells. Metastatic lungs were harvested, and effector-like Tex cells were analyzed by flow cytometry on day 8 post-melanoma cell inoculation. A significant reduction in the frequency of expanded

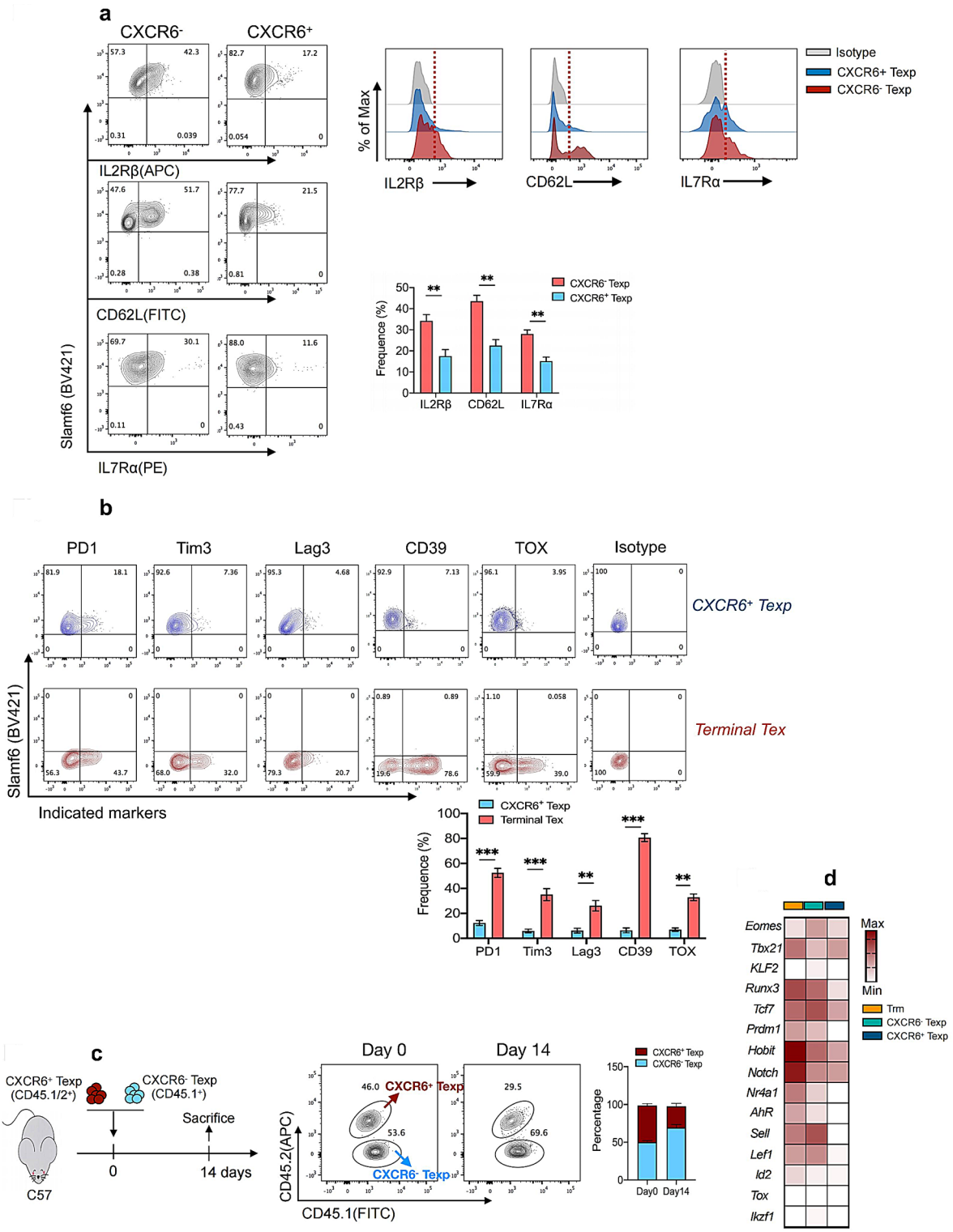


effector-like Tex cells was observed in donors with CXCR6-deficient cells compared to that in their normal counterparts (Fig. 4c). Collectively, these findings suggest that CXCR6$^+$ Texp cells play a crucial role in generating functional CD8$^+$ T cells against tumors within the metastatic microenvironment, while delayed differentiation was observed in their CXCR6$^-$ counterparts.

**Fig. 3** The molecular characteristics associated with memory of Texp cells. C57BL/6J mice were adoptively transferred with $5\times10^5$ of splenic CD45.1$^+$ OT-I cells on day −2, followed by intravenous injection with B16-OVA cells. On day 12 post transfer, lung-derived TILs were isolated and subjected to flow cytometry. (**a**). The representative staining and quantification of IL2Rβ, IL7Rα or CD62L expression on CXCR6$^+$ and CXCR6$^-$ Texp subsets; (**b**). Flow cytometry analysis of inhibitor factors PD-1, Tim3, Lag3, CD39, Tox expression on CXCR6$^+$ Texp cells and terminal Tex cells. Cells were gated from live CD45.1$^+$CD44$^+$ cells. The experiments were performed at least twice with similar results ($n=5$ per group). **c** The schematic of experimental design (left) and the flow cytometry analysis (right) of in vivo co-transfer assay. The Texp cells utilized in the flow cytometry analysis originated from the lung tissue of the host mouse. **d** Heatmap of different gene expressions of antigen-specific OT-I cells by using q-PCR. Mice were adoptively transferred with naïve OT-I cells on day −1 and were intranasally infected with influenza A/HKx31 containing OVA peptide at 300 EID50; then lung tissues were harvested and tissue-resident memory CD8$^+$ T cell (Trm) cells were isolated on day 40 post infection. Lung-infiltrated Texp cells were processed as above described. In (**a**-**b**), statistical comparisons were performed using an unpaired t-test, $^{**}p<0.01$, $^{***}p<0.001$. Data are shown as the mean ± s.e.m. and representative of two independent experiments

### 3.5 CXCR6$^+$ Texp cells exhibit potent control over lung metastasis

To investigate the role of antigen-specific Texp cells in metastasis control, approximately $1\times10^6$ cells were isolated from metastatic lungs and subsequently transferred into pre-established *Cd8*$^{-/-}$ mice with metastases (mice with homogeneous levels of lucifer fluorescence were incorporated into the treatment group) (Fig. 5a). A substantial proportion of donor cells exhibited lung homing following the transfer (supplemental figure S5a). The number of metastatic foci was quantified on day 16 post-adoptive transfer. Mice receiving CXCR6$^+$ Texp cells showed a significant reduction in the number of metastatic foci compared to the other two groups (Fig. 5a). In addition, we evaluated the survival duration of these recipient mice and observed that nearly half of them exhibited a prolonged lifespan of up to 60 days following the transfer of CXCR6$^+$ Texp cells, which was significantly longer than that of the control mice (Fig. 5b). Furthermore, we implemented a combined therapeutic approach involving cellular adoptive transfer and cyclophosphamide (CTX) administration in pre-established lung metastasis-bearing mice. We observed that treatment with CTX alone extended the lifespan of mice; however, when combined with the adoptive transfer of CXCR6$^+$ Texp cells, it significantly enhanced therapeutic efficacy against metastasis (Fig. 5c). However, the effectiveness of adoptive transfer of CXCR6$^+$ Texp cells appears to be limited in the context of targeting subcutaneous tumors (supplemental figure S5b). Collectively, these findings highlight the potential value of Texp cell transfer as a promising therapeutic strategy for effectively managing metastasis.

To investigate the potential impact of CXCR6$^+$ subset deficiency on the suppressive capacity of CD8$^+$ T cells in metastasis, we established a bone marrow chimeric mouse model by combining bone cells derived from C57 donors and *Cxcr6*$^{-/-}$ donors or *Cd8*$^{-/-}$ donors and *Cxcr6*$^{-/-}$ donors, followed by injection of cell mixtures into sub-lethally irradiated *Cd8*$^{-/-}$ recipients. After 10-week remodeling, the recipient mice were challenged with B16-OVA cells. The results revealed that the absence of CXCR6$^+$ subsets failed to confer effective protection against metastasis in mice (supplemental figure S5c).

We performed a therapeutic experiment wherein purified lung-derived Texp cells were adoptively transferred into *Cd8*$^{-/-}$ recipient mice on day −2 after B16-OVA inoculation (Fig. 5d). Transfer of CXCR6$^-$ cells conferred substantial protection against lung metastasis, whereas mice receiving CXCR6$^+$ cell transfer exhibited limited survival. These results indicate that CXCR6$^+$ Texp cells have the capacity to control lung metastasis, while CXCR6$^-$ cells exhibit preventive effects against it.

### 3.6 CXCR6$^+$ Texp cells exert metastasis control through diverse mechanisms

Based on our findings, adoptive transfer of tumor-specific CXCR6$^+$ Texp cells has the potential to mitigate metastasis. We postulated that CXCR6$^+$ Texp cells exert direct cytotoxic effects against tumor cells. To test this hypothesis, naïve CD45.1$^+$ OT-I cells were adoptively transferred into C57 mice, followed by administration of B16-OVA cells. Lung tissues were harvested and expanded CD45.1$^+$ OT-I cells were analyzed using flow cytometry. We observed that CXCR6$^+$ Texp cells exhibited a high expression of the activation-associated marker KLRG1, whereas minimal expression was detected on CXCR6$^-$ cells at day 12 post-cell transfer (Fig. 6a). Moreover, transfer of CXCR6$^+$ Texp cells showed augmented cytotoxicity by upregulating the production of cytokines including IFN-γ, TNFα, CD107a/b, and GzmB, which are associated with cytolytic function (Fig. 6b). To confirm the cytotoxicity of CXCR6$^+$ Texp cells against tumor cells, we performed an in vitro killing assay (supplemental figure S6a). Lung-derived CXCR6$^+$ Texp cells were isolated from metastasis-bearing mice and co-cultured with CFSE-labeled target cells for 12 h, followed by flow cytometry. The attenuation of the fluorescent signal implies that the target cell has been effectively eliminated. Notably, these cells exhibited potent direct cytotoxicity as evidenced by a significant reduction in the target cell population (Fig. 6c). Furthermore, CXCR6$^+$ Texp cells were activated, sorted, and co-cultured with CFSE-labeled B16-OVA cells before being re-transferred into *Cd8*$^{-/-}$ recipient mice. Naïve OT-I cells were used as controls, and apoptosis

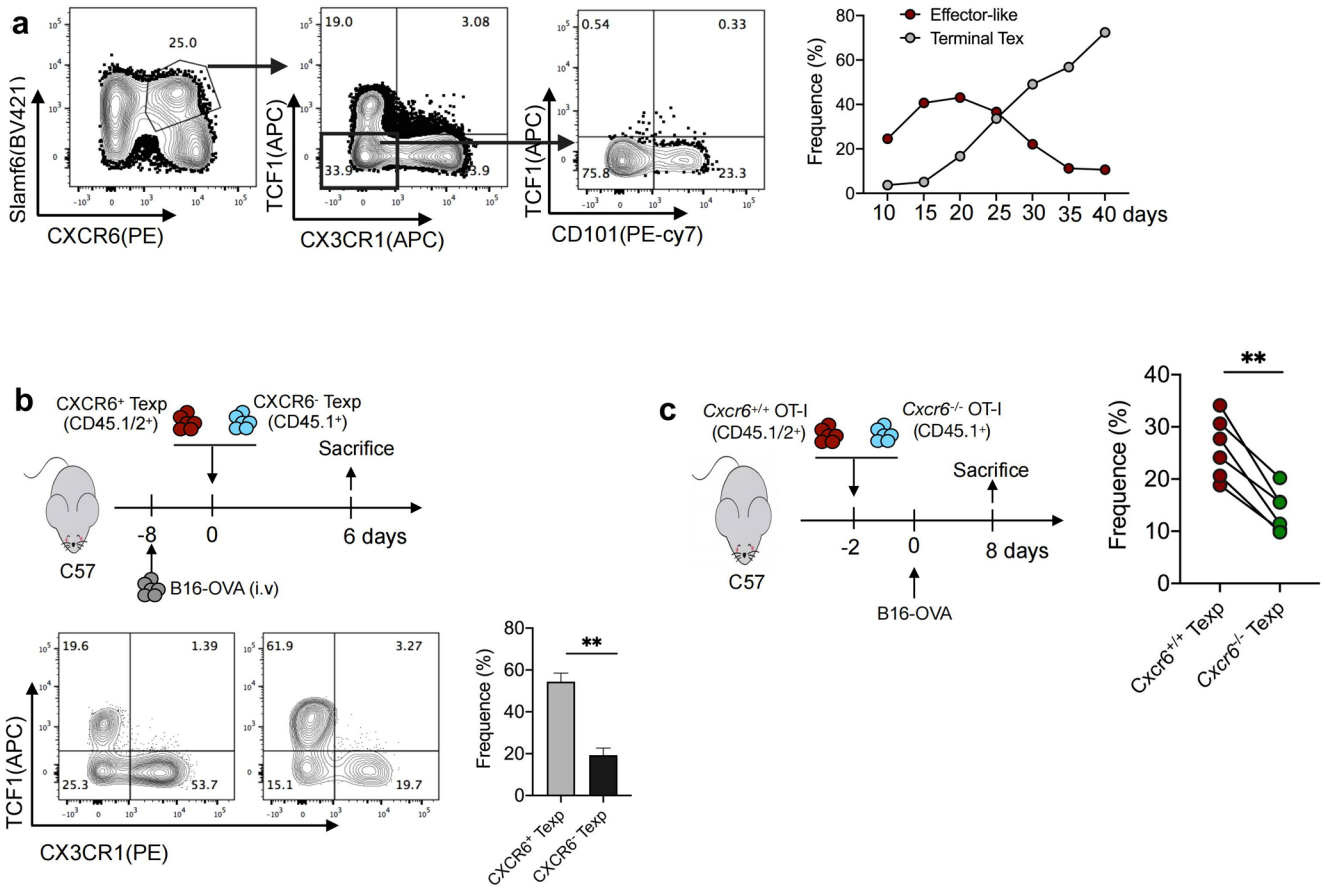


**Fig. 4** CXCR6$^+$ Texp cells served as a crucial source of effector-like Tex cells (**a**). Representative flow cytometry staining (left) and summary (right) of differentiation pattern on effector-like and terminal Tex subsets at different time points. A total of $5\times10^5$ of CD45.1$^+$OT-I cells were adoptively transferred into C57BL/6J mice subsequently intravenous injection with B16-OVA cells. On day 8 post tumor cell inoculation, lung tissues were harvested, and CXCR6$^+$Texp cells were purified and re-transfer into metastasis-matched mice. **b** The flow cytometry analyses of the percentages of TCF1$^-$CX3CR1$^+$ OT-I cells. CD45.1$^+$CXCR6$^-$ and CD45.1/2$^+$CXCR6$^+$ Texp cells were sorted from lungs of metastatic mice on day 8 and were co-transfer in a 1:1 ration (a total of $6\times10^5$) into metastasis-matched mice inoculated with B16-OVA cells ($n=3$ per group) (**c**). The schematics of experimental design of in vivo co-transfer assay. Naïve *Cxcr6* deficient Texp cells were isolated from CD45.1$^+$ background mice, and equally mixed with CD45.1$^+$CD45.2$^+$ normal Texp cells to co-transfer into C57BL/6J mice. Statistical comparisons were performed using an unpaired t-test, $^{**}p<0.01$. Data are shown as the mean±s.e.m. with 6 mice per group and representative of two independent experiments

of melanoma cells in the lungs was evaluated using flow cytometry. Notably, the transfer of CXCR6$^+$ Texp cells significantly increased the percentage of 7-AAD$^+$ annexin V$^+$ melanoma cells in vivo (supplemental figure S6b).

The absolute number of dendritic cell (DC) expressing CD11c and MHCII, which play a crucial role in antigen recognition by CD8$^+$ T cells within the tumor microenvironment, was significantly higher in the lungs of recipient mice following the transfer of CXCR6$^+$ Texp cells than in the control group (supplemental figure S6c). Previous study have demonstrated the substantial presence of bystander CD8$^+$ T cells within tumor infiltrates [31]. Isolated CXCR6$^+$ Texp cells (CD45.1$^+$) were re-transferred into naïve C57 recipients, followed by the administration of B16-OVA cells. On day 16 post-transfer, endogenous CD45.2$^+$CD8$^+$ T cells were sorted and cultured with $OVA_{257-264}$ peptide in vitro. Upon stimulation, a significant increase in the proportion of IFN-gamma-producing CD8$^+$ T cells was observed among mice that received a transfer of CXCR6$^+$ Texp cells, indicating the augmented presence of tumor-reactive CD8$^+$ T cells (Fig. 6d) (supplemental figure S6d).

### 3.7 CXCR6$^+$ Texp cells can respond to ICB

Cancer immunotherapy involving ICB with monoclonal antibodies targeting PD-1/PD-L1 has demonstrated the ability to restore the impaired function of cytotoxic effector CD8$^+$ T cells, resulting in tumor regression and prolonged patient survival [8, 32, 33]. However, the subsets of CD8$^+$ T cells that respond to ICB in tumors remain elusive. Based on our findings, a minority of tumor-specific CXCR6$^+$ Texp cells exhibit PD1 protein expression during metastasis,

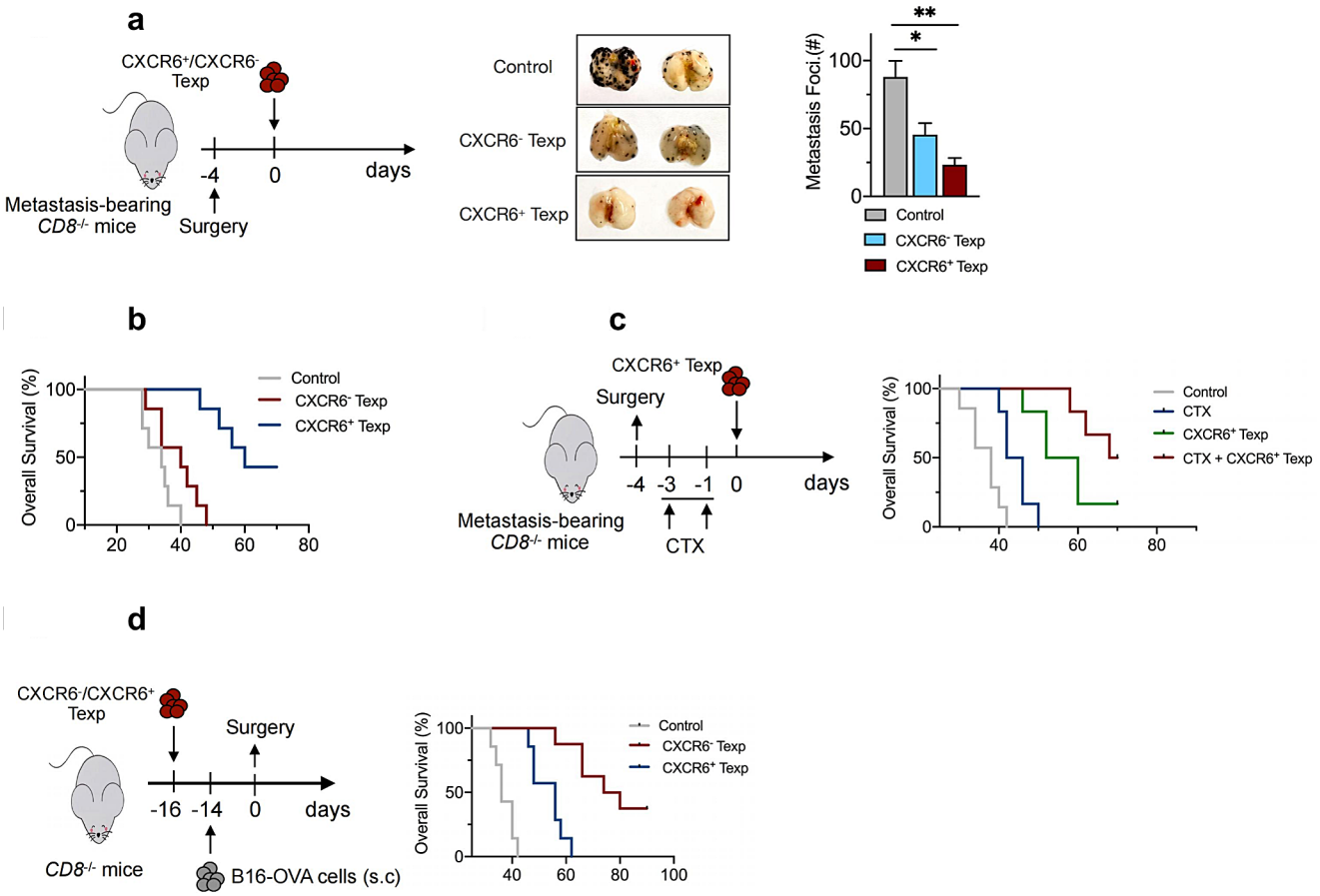


**Fig. 5** CXCR6 + Texp cells effectively mitigated lung metastasis (**a**-**d**). The schematics of experimental design of in vivo cell-transfer immunotherapy assay and survival curves of control or treated mice. No treatment mice was used as control. Log rank test of survival data was used. Approximately $1 \times 10^6$ of lung-derived CXCR6$^-$/CXCR6$^+$ Texp cells were sorted from metastatic donor mice on day 12 as above described. Cells were adoptively transferred into pre-established metastasis-bearing *Cd8*$^{-/-}$ mice 4 days post-surgery, respectively. The representative images of lung nodules (**a**) or survival curve (**b**) of mice were measured. Red line versus gray line, $p = 0.068$; Blue line versus Red line, $p < 0.01$. **c** The recipient mice were administrated with cyclophosphamide (CTX, sigma) drug at a dose of 350 mg/kg i.p. twice prior to CXCR6$^+$ Texp cells transfer ($1 \times 10^6$). Green line versus blue line, $p < 0.05$; Red line versus blue line, $p < 0.01$; Red line versus green line, $p < 0.05$. **d** A total of $1 \times 10^6$ of CXCR6$^-$/CXCR6$^+$ Texp cells were adoptively transferred into C57BL/6J mice subsequently subcutaneous footpad inoculation with B16-OVA cells ($1 \times 10^6$). Blue line versus gray line, $p < 0.01$; Red line versus blue line, $p < 0.01$.In (**a**), statistical comparisons were performed using an unpaired t-test, *$p < 0.05$, **$p < 0.01$. Data are shown as the mean ± s.e.m. with 4–7 mice per group and representative of two independent experiments

indicating their potential responsiveness to ICB. To test this hypothesis, we isolated lung-derived CXCR6$^+$ Texp cells from metastasis-bearing mice and cultured them with an anti-PD1 antibody in vitro along with anti-CD3 and anti-CD28 antibodies. After treatment with the anti-PD1 antibody, there was a two-fold increase in the absolute number of Texp cells, indicating that antigen-specific CXCR6$^+$ Texp cells responded to the PD1 blockade (Fig. 7a). To confirm this observation, we transferred isolated CXCR6$^+$ Texp cells into pre-established metastatic mice and administered three doses of anti-PD1, while monitoring cell proliferation using BrdU dye. A significant increase in donor-derived BrdU$^+$ cells was observed following anti-PD1 treatment (Fig. 7b). However, endogenous tumor-specific CD8$^+$ T cells exhibited a slight upregulation of BrdU expression (supplemental figure S7a). Collectively, these findings demonstrate the capacity of CXCR6$^+$ Texp cells to respond to ICB and potentially enhance the therapeutic efficacy of ACT.

To investigate the potential synergistic effect of the adoptive transfer of tumor-specific CXCR6$^+$ Texp cells in combination with ICB, we adoptively transferred these cells into metastasis-bearing *Cd8*$^{-/-}$ mice prior to the administration of anti-PD1 antibodies. Combination therapy involving CXCR6$^+$ Texp cells and anti-PD1 blockade demonstrated superior therapeutic efficacy compared to individual treatments in our study (Fig. 7c).

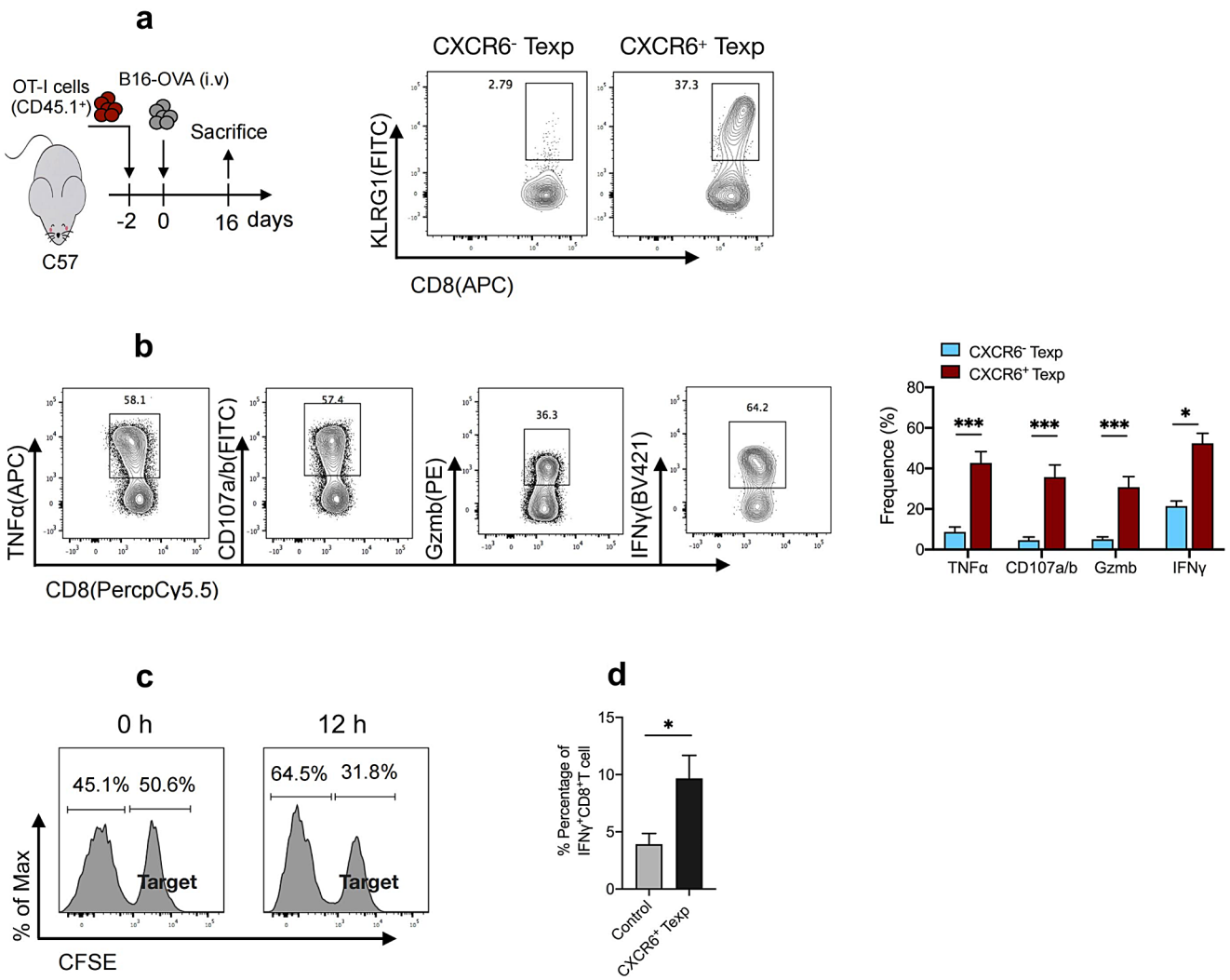


**Fig. 6** CXCR6$^+$ Texp cells exerted direct cytotoxic effects on tumor cells. (**a-b**) Approximately $5\times10^5$ of splenic CD45.1$^+$ OT-I cells were transferred into C57BL/6J mice ($n=4$ per group) subsequently intravenous injection with $3\times10^5$ of B16-OVA cells. On day 12 post transfer, lungs were harvested and TILs were processed to flow cytometry. Flow cytometry analyzing KLRG1 expression (**a**), or granzyme B(Gzmb), CD107a/b, tumor necrosis factor-α (TNFα) and IFNγ expressions (**b**), on CXCR6$^-$/CXCR6$^+$ Texp cells. (**c**). Flow cytometry data of the in vitro killing capacity assay of CXCR6$^+$ Texp cells. The details as shown in methods and supplemental figure S6a. **(d).** Flow cytometry analyzing the frequency of IFNγ$^+$CD8$^+$ T cells after in vitro stimulation with $OVA_{257-264}$ peptide along with PMA, ionomycin and GolgiPlug/stop for 5 hours. The assay design as shown in supplemental figure S6d. In (**b**, **d**) statistical comparisons were performed using an unpaired t-test, $*p<0.05$, $***p<0.001$. Data are shown as the mean±s.e.m. and representative of two independent experiments

## 4 Discussion

In this study, we used lung metastasis as a research model and identified CXCR6$^+$ Texp cells as crucial contributors to anti-tumor metastasis. The underlying mechanisms are multifaceted: first, CXCR6$^+$ Texp cells can directly differentiate into effector-like CD8$^+$ T cells; second, these cells possess the ability to secrete cytotoxic cytokines, which has been validated through in vitro and in vivo killing experiments, demonstrating their direct tumor cell-killing capacity; third, CXCR6$^+$ Texp cells can recruit tumor-reactive CD8$^+$ T cells to participate in anti-metastasis responses by potentially mobilizing helper immune cells such as DCs. Recent reports have also corroborated the indispensable role of CXCR6$^+$CD8$^+$ T cells in the anti-tumor process [34, 35]. Building on these findings, our study is first to elucidate the immunological characteristics of CXCR6-expressing Texp cells in metastatic tumor tissues, including their phenotypic expression, differentiation profiles, and functional analysis. This study enriches our understanding of the heterogeneity in Tex cells and sheds light on potential strategies for treating metastases, providing novel insights into clinical tumor immunotherapy.

TCF1 and Slamf6 exhibited strong co-expression on tumor-reactive CD8$^+$ T cells in the lungs, supporting the notion that Slamf6 serves as a unique molecule for Texp

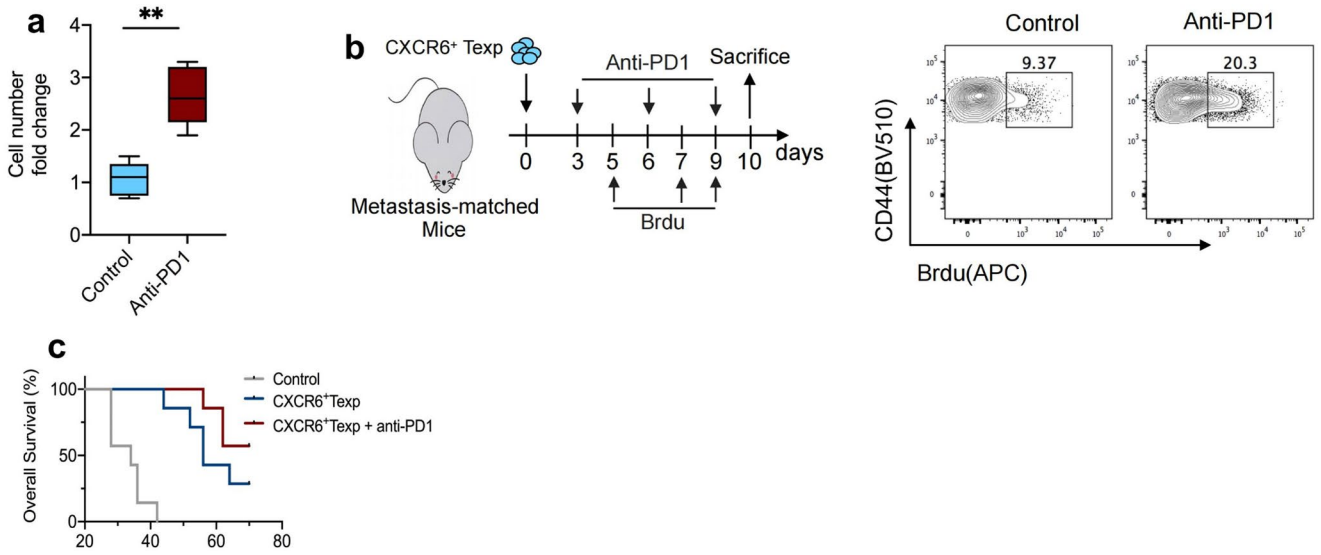


**Fig. 7** CXCR6$^+$Texp cells could respond to immune checkpoint blockade (**a**). Flow cytometry analyzing absolute number of CXCR6$^+$Texp cells which were isolated from metastatic mice on day 8 post cell transfer, followed by in vitro stimulation with IL2 and anti-PD1 mAb in CD3/CD28 mAbs-coated culture plates for 72 h. (**b**). The assay design of in vivo anti-PD1 mAb treatment and the representative flow cytometry staining of Brdu on CD44$^+$CD45.1$^+$CXCR6$^+$Texp cells in metastasis-matched mice. (**c**). Approximately $1 \times 10^6$ of CXCR6$^+$Texp cells as described in (**a**) were adoptively transferred into metastasis-bearing *Cd8*$^{-/-}$ mice. Recipient mice were administrated with anti-PD-1 or control antibody at dose of 6 mg/kg on 5, 8, 11 days post cell transfer. No treatment mice was used as control. Survival curves of mice were calculated. Log rank test was used. Blue line versus gray line, $p < 0.01$; Red line versus blue line, $p = 0.037$

cells [12]. Therefore, we identified Slamf6$^+$Tim3$^-$ cells as tumor-specific Texp cells in this study. Based on their distinct surface marker expression profiles, we categorized antigen-specific CD8$^+$ T cells into precursor, effector-like, and terminal Tex cells. Among these subsets, Texp cells initially emerged as the predominant subgroup, likely due to their low tumor antigen burden. Notably, adoptive transfer of Texp cells to mid-term metastasis-bearing mice did not confer a significant survival advantage. This observation may be attributed to the inhibitory tumor microenvironment, which impairs the differentiation or cytotoxic function of the transferred cells. Previous studies have suggested the occurrence of irreversible epigenetic alterations, known as epigenetic scarring, even in the early development of Texp cells compared to memory cells [36, 37]. In this study, we found that Texp cells maintain cellular stemness in metastatic tissues, particularly CXCR6$^-$ cells, which exhibit high expression levels of memory-specific surface molecules such as IL2Rβ, IL7Rα, CD62L; however, CXCR6$^+$ cells exhibit partial loss of these characteristics. These findings underscore the presence of cellular heterogeneity within Texp cells during metastasis.

CXCR6$^+$ cells exhibited characteristics resembling a subset of later-stage differentiated Texp cells, owing to their rapid response to antigen stimulation and intrinsic expression of KLRG1. Functional memory CD8$^+$ T cells can produce various inflammatory effector cytokines such as IFN-γ, TNF-α, and Gzmb. Upon re-encountering cognate antigens, they undergo lytic degranulation, which may serve as an important mechanism by which CXCR6$^+$ Texp cells control metastasis. Furthermore, tumor cells themselves are capable of expressing CXCL16, which is a chemokine targeting CXCR6 receptors and mediating the migration of various types of T lymphocytes, including CXCR6$^+$ Texp cells, within the tumor microenvironment. Consequently, the administration of additional CXCL16 agents might enhance the therapeutic efficacy of ACT; however, this could also be a double-edged sword, as CXCL16 has been reported to potentially facilitate the proliferation of tumor cells [38]. Our in vivo re-infusion experiment revealed that the early transfer of CXCR6$^+$ Texp cells exerts a significant control over lung metastasis, while CXCR6$^-$ cells exhibit a certain preventive effect on it. Consequently, we aim to conduct further studies on the anti-metastatic function of CXCR6$^-$ Texp cells with the aim of long-term prevention of tumor recurrence following surgical procedures or chemotherapy.

FTY720 is an immune-modulating drug that induces lymphopenia without influencing T cell activation and proliferation [39]. The potential mechanism underlying this is that it functions as a potent agonist at four sphingosine 1-phosphate receptors of lymphocytes, arising from a reversible redistribution [40]. Our research findings indicate that draining lymph nodes constitute an essential source of CXCR6$^+$ Texp cells, and a notable decrease in the pulmonary infiltration of CXCR6$^+$ Texp cells was witnessed subsequent to FTY720 treatment. Recent reports have highlighted the pivotal role

of tumor-draining lymph nodes in anti-tumor immunity [41, 42]. Therefore, isolating and transfusing this cell population from the lymph nodes could represent a viable strategy against tumor metastasis. It should be noted that this study mainly focused on metastasis in the lung tissue; however, the applicability of these findings to other tissues remains unknown, which also represents a future research direction.

Effector-like Tex cells have been reported to possess tumoricidal activity and are considered crucial functional cells involved in tumor control. Compared to the group without cell transfusion, the transfer of effector-like Tex cells significantly prolonged the survival time of mice. However, unlike antigen-specific $CD8^+$ T cells activated in vitro, effector-like Tex cells within metastatic tissues failed to effectively control metastasis (Fig. 1b and d). This phenomenon may be attributed to the inhibitory tumor microenvironment, in which effector-like Tex cells lose their effector characteristics and cannot be promptly replenished, resulting in transient and limited cytotoxic effects. In contrast, our findings (Fig. 1d) demonstrated that the transfer of an equivalent number of effector-like Tex cells resulted in a survival rate comparable to that of terminal Tex cells in mice, suggesting that terminal Tex cells did not completely lose their anti-tumor functionality in metastasis, in line with the conclusion of a previous study [43–45].

Blockade of the PD-1/PD-L1 pathway has demonstrated remarkable efficacy in clinical tumors that are resistant to conventional therapeutic modalities, including surgery, radiation, and chemotherapy [46–49]. The potential mechanism underlying this phenomenon is that PD-L1 can effectively facilitate the crosslinking of PD1 and induce immunosuppression in effector T cells by recruiting tyrosine protein phosphatase SHP2 to the cytoplasmic domain of PD1, where it dephosphorylates proximal signals from the T-cell receptor and CD28 [50, 51]. However, a large proportion of patients do not experience long-term benefits because of the inherent heterogeneity of $CD8^+$ T cells, resulting in unpredictable responses. Early studies suggested that the inhibitory effect of the PD1 blockade primarily targeted terminal Tex cells; however, recent reports have highlighted the presence of irreversible epigenetic alterations in these cells [52, 53]. The specific subset of $CD8^+$ T cells within the tumor microenvironment that responds to anti-PD1 antibodies remains unidentified; however, our data demonstrated a significant expansion of $CXCR6^+$ Texp cells upon PD1 treatment, indicating their potential for ICB response. This suggests that the combined application of cell transfusion and anti-PD1 antibodies may prevent metastasis or recurrence. Further investigations are warranted to explore whether PD1 treatment induces alterations in the immunological characteristics of $CXCR6^+$ Texp cells, including epigenetic modifications, phenotypic changes, and differentiation status.

The chemotherapeutic agent CTX is widely used in clinical oncology for cancer treatment. However, CTX is also an immunosuppressant [54]. Thus, in the ACT combined with CTX immunotherapeutic experiment, it was necessary to administer CTX first and subsequently transfer the $CXCR6^+$ Texp cells, in order to preclude the possibility that CTX might cause damage to the infusion cells. In this experiment, we observed that CTX monotherapy effectively controlled metastasis within a short duration. This therapeutic effect was further enhanced when combined with cell transfusion, suggesting a potential clinical treatment strategy for metastasis. However, the underlying mechanism remains elusive. One plausible explanation is that CTX initially targets chemosensitive tumor cells. Considering the nonselective inhibition of endogenous cells, our standard protocol involves administration of CTX prior to cell infusion.

In conclusion, this study enhanced our understanding of the heterogeneity of Tex cells in metastatic tumor tissues, thereby facilitating an alternative therapeutic strategy. Further investigations are warranted to elucidate the underlying anti-metastatic mechanisms to achieve prolonged remission in patients with metastatic tumors when combined with conventional treatments in clinical settings.

**Supplementary Information** The online version contains supplementary material available at https://doi.org/10.1007/s13402-025-01040-1.

**Acknowledgements** We thank Professor Luo for her invaluable guidance in experimental design, we thank Fudan University Experimental Animal Center for their invaluable assistance in establishing the mouse model, and we thank the School of Basic Medicine of Fudan University for cell sorting.

**Author contributions** YS, JC, YQZ carried out the animal and cell experiments; NW, YJZ, GC, FM participated in the immunoassays. YS, ZC participated in the design of the study and performed the statistical analysis. YQW supervised the study, and participated in its design and coordination and helped to draft the manuscript. All authors read and approved the final manuscript.

**Funding** This work was supported by Science Foundation of Shanghai Health Commission, Grant/ Award Number: 20204Y0484.

**Data availability** No datasets were generated or analysed during the current study.

## Declarations

**Ethics approval and consent to participate** All mouse experiments were performed in accordance with the guidelines of the Department of Laboratory Animal Science of the Fudan University (Approval Number: 2024-HSYY-716).

**Competing interests** The authors declare no competing interests.

## References

1. S. Valastyan, R.A. Weinberg, Tumor metastasis: molecular insights and evolving paradigms. Cell. **147**, 275–292 (2011). https://doi.org/10.1016/j.cell.2011.09.024
2. M.E. Dudley et al., Cancer regression and autoimmunity in patients after clonal repopulation with antitumor lymphocytes. Science. **298**, 850–854 (2002). https://doi.org/10.1126/science.1076514
3. J.J. Hong et al., Successful treatment of melanoma brain metastases with adoptive cell therapy. Clin. Cancer Res. **16**, 4892–4898 (2010). https://doi.org/10.1158/1078-0432.CCR-10-1507
4. A. Gros et al., PD-1 identifies the patient-specific CD8(+) tumor-reactive repertoire infiltrating human tumors. J. Clin. Invest. **124**, 2246–2259 (2014). https://doi.org/10.1172/JCI73639
5. P.S. Kim, R. Ahmed, Features of responding T cells in cancer and chronic infection. Curr. Opin. Immunol. **22**, 223–230 (2010). https://doi.org/10.1016/j.coi.2010.02.005
6. T. Zenz, Exhausting, T cells in CLL. Blood. **121**, 1485–1486 (2013). https://doi.org/10.1182/blood-2013-01-475939
7. L.M. McLane, M.S. Abdel-Hakeem, E.J. Wherry, CD8 T cell exhaustion during chronic viral infection and Cancer. Annu. Rev. Immunol. **37**, 457–495 (2019). https://doi.org/10.1146/annurev-immunol-041015-055318
8. S.L. Topalian et al., Safety, activity, and immune correlates of anti-PD-1 antibody in cancer. N Engl. J. Med. **366**, 2443–2454 (2012). https://doi.org/10.1056/NEJMoa1200690
9. A. Addeo, G.L. Banna, G. Metro, Di M. Maio, Chemotherapy in Combination with Immune Checkpoint inhibitors for the First-Line treatment of patients with Advanced Non-small Cell Lung Cancer: a systematic review and literature-based Meta-analysis. Front. Oncol. **9**, 264 (2019). https://doi.org/10.3389/fonc.2019.00264
10. B.C. Creelan et al., Tumor-infiltrating lymphocyte treatment for anti-PD-1-resistant metastatic lung cancer: a phase 1 trial. Nat. Med. **27**, 1410–1418 (2021). https://doi.org/10.1038/s41591-021-01462-y
11. B.C. Miller et al., Subsets of exhausted CD8(+) T cells differentially mediate tumor control and respond to checkpoint blockade. Nat. Immunol. **20**, 326–336 (2019). https://doi.org/10.1038/s41590-019-0312-6
12. W.H. Hudson et al., Proliferating transitory T cells with an effector-like transcriptional signature emerge from PD-1(+) stem-like CD8(+) T cells during chronic infection. Immunity. **51**(e1044), 1043–1058 (2019). https://doi.org/10.1016/j.immuni.2019.11.002
13. J.C. Beltra et al., Developmental Relationships of Four Exhausted CD8(+) T Cell Subsets Reveals Underlying Transcriptional and Epigenetic Landscape Control Mechanisms. Immunity. **52**, 825–841 e828. (2020) https://doi.org/10.1016/j.immuni.2020.04.014
14. Z. Chen et al., TCF-1-Centered Transcriptional Network Drives an Effector versus Exhausted CD8 T Cell-Fate Decision. Immunity. **51**, 840–855 e845. (2019) https://doi.org/10.1016/j.immuni.2019.09.013
15. D.T. Utzschneider et al., Early precursor T cells establish and propagate T cell exhaustion in chronic infection. Nat. Immunol. **21**, 1256–1266 (2020). https://doi.org/10.1038/s41590-020-0760-z
16. J.R. Giles et al., Shared and distinct biological circuits in effector, memory and exhausted CD8(+) T cells revealed by temporal single-cell transcriptomics and epigenetics. Nat. Immunol. **23**, 1600–1613 (2022). https://doi.org/10.1038/s41590-022-01338-4
17. I. Siddiqui et al., Intratumoral Tcf1(+)PD-1(+)CD8(+) T cells with stem-like Properties promote Tumor Control in Response to Vaccination and Checkpoint Blockade Immunotherapy. Immunity. **50**(e110), 195–211 (2019). https://doi.org/10.1016/j.immuni.2018.12.021
18. S. Kurtulus et al., Checkpoint Blockade Immunotherapy Induces Dynamic Changes in PD-1(-)CD8(+) Tumor-Infiltrating T Cells. Immunity 50, 181–194 e186. https://doi.org/10.1016/j.immuni.2018.11.014 (2019)
19. R. Giavazzi, A. Decio, Syngeneic murine metastasis models: B16 melanoma. Methods Mol. Biol. **1070**, 131–140 (2014). https://doi.org/10.1007/978-1-4614-8244-4_10
20. R. He et al., Follicular CXCR5- expressing CD8(+) T cells curtail chronic viral infection. Nature. **537**, 412–428 (2016). https://doi.org/10.1038/nature19317
21. S.J. Im et al., Defining CD8+T cells that provide the proliferative burst after PD-1 therapy. Nature. **537**, 417–421 (2016). https://doi.org/10.1038/nature19330
22. Y.A. Leong et al., CXCR5(+) follicular cytotoxic T cells control viral infection in B cell follicles. Nat. Immunol. **17**, 1187–1196 (2016). https://doi.org/10.1038/ni.3543
23. J. Brummelman et al., High-dimensional single cell analysis identifies stem-like cytotoxic CD8(+) T cells infiltrating human tumors. J. Exp. Med. **215**, 2520–2535 (2018). https://doi.org/10.1084/jem.20180684
24. J.M. Ubellacker et al., Lymph protects metastasizing melanoma cells from ferroptosis. Nature. **585**, 113–118 (2020). https://doi.org/10.1038/s41586-020-2623-z
25. J. Rotman, B.D. Koster, E.S. Jordanova, A.M. Heeren, de Gruijl, T. D. Unlocking the therapeutic potential of primary tumor-draining lymph nodes. Cancer Immunol. Immunother. **68**, 1681–1688 (2019). https://doi.org/10.1007/s00262-019-02330-y
26. F. Dammeijer et al., The PD-1/PD-L1-Checkpoint Restrains T cell Immunity in Tumor-Draining Lymph Nodes. Cancer Cell 38, 685–700 e688. https://doi.org/10.1016/j.ccell.2020.09.001 (2020)
27. J.R. Giles, A.M. Globig, S.M. Kaech, E.J. Wherry, CD8(+) T cells in the cancer-immunity cycle. Immunity. **56**, 2231–2253 (2023). https://doi.org/10.1016/j.immuni.2023.09.005
28. T. Gebhardt, S.L. Park, I.A. Parish, Stem-like exhausted and memory CD8(+) T cells in cancer. Nat. Rev. Cancer. **23**, 780–798 (2023). https://doi.org/10.1038/s41568-023-00615-0
29. S.M. Kaech, E.J. Wherry, Heterogeneity and cell-fate decisions in effector and memory CD8+T cell differentiation during viral infection. Immunity. **27**, 393–405 (2007). https://doi.org/10.1016/j.immuni.2007.08.007
30. J.T. Harty, V.P. Badovinac, Shaping and reshaping CD8+T-cell memory. Nat. Rev. Immunol. **8**, 107–119 (2008). https://doi.org/10.1038/nri2251
31. Y. Simoni et al., Bystander CD8(+) T cells are abundant and phenotypically distinct in human tumour infiltrates. Nature. **557**, 575–579 (2018). https://doi.org/10.1038/s41586-018-0130-2

32. W. Zou, J.D. Wolchok, L. Chen, PD-L1 (B7-H1) and PD-1 pathway blockade for cancer therapy: mechanisms, response biomarkers, and combinations. Sci. Transl Med. **8**, 328rv324 (2016). https://doi.org/10.1126/scitranslmed.aad7118
33. Y. Jiang, X. Zhao, J. Fu, H. Wang, Progress and challenges in Precise Treatment of Tumors with PD-1/PD-L1 blockade. Front. Immunol. **11**, 339 (2020). https://doi.org/10.3389/fimmu.2020.00339
34. Di M. Pilato et al., CXCR6 positions cytotoxic T cells to receive critical survival signals in the tumor microenvironment. Cell 184, 4512–4530 e4522. https://doi.org/10.1016/j.cell.2021.07.015 (2021)
35. A.K. Molodtsov et al., Resident memory CD8(+) T cells in regional lymph nodes mediate immunity to metastatic melanoma. Immunity 54, 2117–2132 e2117. https://doi.org/10.1016/j.immuni.2021.08.019 (2021)
36. D.R. Sen et al., The epigenetic landscape of T cell exhaustion. Science. **354**, 1165–1169 (2016). https://doi.org/10.1126/science.aae0491
37. K.E. Pauken et al., Epigenetic stability of exhausted T cells limits durability of reinvigoration by PD-1 blockade. Science. **354**, 1160–1165 (2016). https://doi.org/10.1126/science.aaf2807
38. J. Korbecki et al., The role of CXCL16 in the pathogenesis of Cancer and Other diseases. Int. J. Mol. Sci. **22** (2021). https://doi.org/10.3390/ijms22073490
39. D.D. Pinschewer et al., FTY720 immunosuppression impairs effector T cell peripheral homing without affecting induction, expansion, and memory. J. Immunol. **164**, 5761–5770 (2000). https://doi.org/10.4049/jimmunol.164.11.5761
40. V. Brinkmann et al., The immune modulator FTY720 targets sphingosine 1-phosphate receptors. J. Biol. Chem. **277**, 21453–21457 (2002). https://doi.org/10.1074/jbc.C200176200
41. K.A. Connolly et al., A reservoir of stem-like CD8(+) T cells in the tumor-draining lymph node preserves the ongoing antitumor immune response. Sci. Immunol. **6**, eabg7836 (2021). https://doi.org/10.1126/sciimmunol.abg7836
42. J.M. Schenkel et al., Conventional type I dendritic cells maintain a reservoir of proliferative tumor-antigen specific TCF-1(+) CD8(+) T cells in tumor-draining lymph nodes. Immunity. **54**, 2338–2353 e2336. (2021) https://doi.org/10.1016/j.immuni.2021.08.026
43. M.A. Paley et al., Progenitor and terminal subsets of CD8+T cells cooperate to contain chronic viral infection. Science. **338**, 1220–1225 (2012). https://doi.org/10.1126/science.1229620
44. E.J. Wherry, J.N. Blattman, K. Murali-Krishna, van der R. Most, R. Ahmed, Viral persistence alters CD8 T-cell immunodominance and tissue distribution and results in distinct stages of functional impairment. J. Virol. **77**, 4911–4927 (2003). https://doi.org/10.1128/jvi.77.8.4911-4927.2003
45. S.D. Blackburn et al., Tissue-specific differences in PD-1 and PD-L1 expression during chronic viral infection: implications for CD8 T-cell exhaustion. J. Virol. **84**, 2078–2089 (2010). https://doi.org/10.1128/JVI.01579-09
46. S.L. Topalian, C.G. Drake, D.M. Pardoll, Immune checkpoint blockade: a common denominator approach to cancer therapy. Cancer Cell. **27**, 450–461 (2015). https://doi.org/10.1016/j.ccell.2015.03.001
47. A. Ribas, J.D. Wolchok, Cancer immunotherapy using checkpoint blockade. Science. **359**, 1350–1355 (2018). https://doi.org/10.1126/science.aar4060
48. V.P. Balachandran et al., Identification of unique neoantigen qualities in long-term survivors of pancreatic cancer. Nature. **551**, 512–516 (2017). https://doi.org/10.1038/nature24462
49. J.D. Wolchok et al., Nivolumab plus Ipilimumab in advanced melanoma. N Engl. J. Med. **369**, 122–133 (2013). https://doi.org/10.1056/NEJMoa1302369
50. T. Yokosuka et al., Programmed cell death 1 forms negative costimulatory microclusters that directly inhibit T cell receptor signaling by recruiting phosphatase SHP2. J. Exp. Med. **209**, 1201–1217 (2012). https://doi.org/10.1084/jem.20112741
51. E. Hui et al., T cell costimulatory receptor CD28 is a primary target for PD-1-mediated inhibition. Science. **355**, 1428–1433 (2017). https://doi.org/10.1126/science.aaf1292
52. M. Philip et al., Chromatin states define tumour-specific T cell dysfunction and reprogramming. Nature. **545**, 452–456 (2017). https://doi.org/10.1038/nature22367
53. H.E. Ghoneim et al., De Novo Epigenetic Programs Inhibit PD-1 Blockade-Mediated T Cell Rejuvenation. Cell. **170**, 142–157 e119. (2017) https://doi.org/10.1016/j.cell.2017.06.007
54. A. Emadi, R.J. Jones, R.A. Brodsky, Cyclophosphamide and cancer: golden anniversary. Nat. Rev. Clin. Oncol. **6**, 638–647 (2009). https://doi.org/10.1038/nrclinonc.2009.146